Chapter 18
Micromirrors

Roberto Carminati and Sonia Costantini

18.1   Application Fields

Micromirrors are among the oldest kind of MEMS solutions which were investigated: the first publication about micromirror devices is traced back to the 1980 [1]. Among the different applications which drove the earlier interest in this type of technology, we can find confocal microscopy, laser printing, bar code reading, switching and interconnection in optical communications.

Micromirror devices were also between the first MEMS to reach high-volume production in consumer market with Texas Instruments' Digital Micromirror Device (DMD) [2]. This device found wide application into light projectors, where the MEMS mirror is used to decide which pixel of the projected image to be on or off. In this case, the micromirror device is composed by a rectangular array of very small (~10 μm $\times$ 10 μm) aluminium mirrors which can stay at rest (ON-state) or be selectively activated to tilt in a position where light does not come out anymore from the projector (OFF-state), as illustrated in Fig. 18.1. The name *Digital* Micromirror Device is related to this binary operation. Another peculiarity of this solution is that the whole image is projected by the MEMS mirror and the size of its mirror elements determines the maximum projection resolution because it corresponds to the image pixel.

R. Carminati (✉)
ST Microelectronics, Analog MEMS and Sensors Group, MEMS Technology and Design R&D, Cornaredo, Italy
e-mail: roberto.carminati@st.com

S. Costantini
ST Microelectronics, Analog MEMS and Sensors Group, MEMS Technology and Design R&D, Agrate Brianza, Monza Brianza, Italy
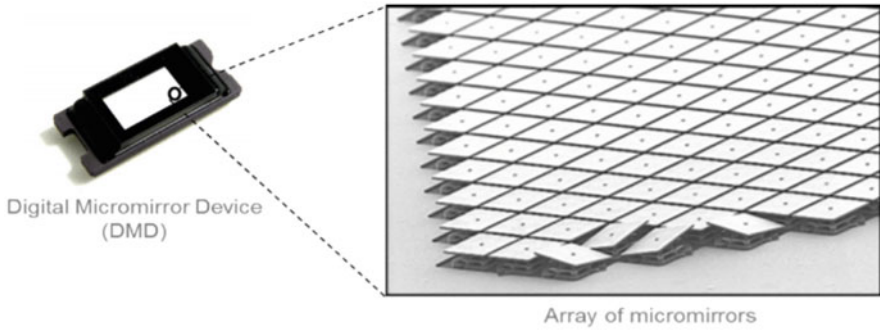e-mail: sonia.costantini@st.com

Fig. 18.1 Digital micromirror device with close-up of mirror array [3]. (Courtesy Texas Instruments)
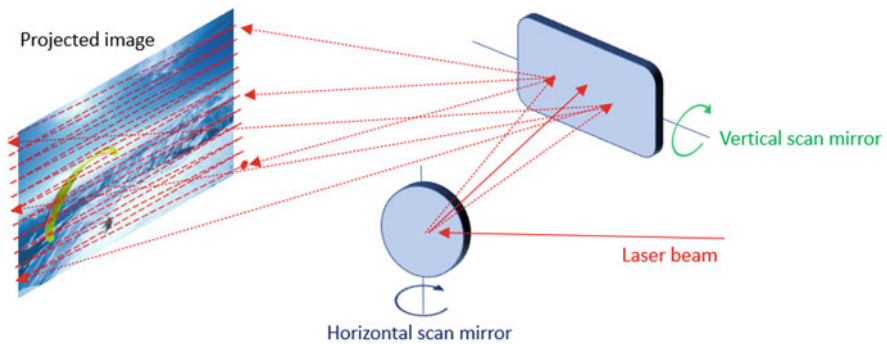

Fig. 18.2 Laser beam scanning display scheme

Such projection concept shows some limitations in scaling into smaller portable applications due to its intrinsically bulky components (light lamp, large micromirror chip to support large resolution). An alternative projector solution has been found in laser beam scanning displays [4], which are based on the generation of an image pixel by pixel through a laser spot which is moved sequentially into different positions. Also, this kind of solution rely on micromirror devices, where in this case only one moving mirror is needed because only one pixel is projected at a time, but where the dimensions of the moving mirror must be quite large (≥ 1 mm) to allow sufficiently small imaged spots on the projection screen and where mechanical scanning angles must be quite large ($\geq 8°$–$10°$) to support an acceptable Field of View (FOV).

A schematic representation of a laser beam scanning display is reported in Fig. 18.2, where a system composed by two mirrors is represented, one for the horizontal scanning and the other for the vertical scanning.

Because in this case the micromirror need to project a laser spot at each pixel position, many hundreds of different positions must be accessible so that practically a continuous scanning micromirror is required: we could then call this kind of design an *analog* micromirror, in contrast to the digital micromirror design previously described.
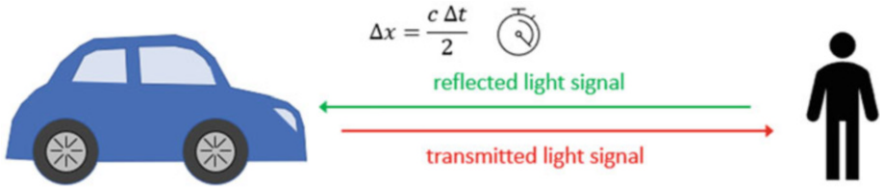
Fig. 18.3 LiDAR working principle. The distance Δx to an object is estimated measuring the time interval Δt between the emission of the light beam and its return, knowing light velocity c

The typical laser beam scanning projector application has a horizontal resolution N_H, which is then related to the mirror scanning angle θ and limited by the diffraction effect on the mirror, whereas the vertical resolution N_V is limited by the scanning rate ratio between the two axes of movement required to project an image [4]:

$$N_H \propto \frac{\theta D}{\lambda}$$

$$N_V \propto \frac{f_H}{f_V.}$$

where D is the mirror diameter, λ is the wavelength of the reflected light, f_H is the scanning frequency for the horizontal image direction and f_V is the frequency of scanning of the vertical image direction.

The advantage of this solution is that it can allow to reach more compact projector dimensions thanks to its smaller components and so it is particularly suited for handheld and wearable devices. Laser beam scanning found commercial application into portable projectors [5] and recently attracts lots of interest in the augmented reality glasses market [6].

In recent years, the research for micromirror application into automotive markets has also increased, driven by the push for autonomous driving and the growing interest for LiDAR (light detection and ranging) sensors. LiDAR is the ranging technology working in the infrared light spectrum and complementary to RADAR. As the RADAR, LiDAR sends off an electromagnetic wave (in this case in the infrared light wavelength range) and estimates distance of an object by measuring the time passing between the wave firing and the reflected echo return. A scheme of this working principle is reported in Fig. 18.3.

LiDAR offers some advantages in terms of range and immunity to atmospheric conditions, and it is considered a mandatory component for the sensing requirements needed to reach full autonomous driving. In such regards, currently available LiDAR adopt macro-mechanical scanning mirrors which are anyway costly, bulky and not always meeting the automotive market reliability standards. Therefore, a lot of companies are looking into inexpensive substitute components to these macro-mechanical mirrors and MEMS mirrors appear as the most natural can-

didates, thanks to their low cost, small dimensions and intrinsic reliability of silicon-based MEMS. As of today, anyway, R&D activity is this field is still ongoing and still no reference architecture based on micromirrors has reached the market.

Additional information on the different kind of applications for MEMS mirrors can be found in [7].

18.2 Types of Micromirrors

In the following, the focus will be on the *analog micromirrors*, composed by a single moving mirror able to rotate in a controllable way along one or more directions. In analogy to motors, the rotating mass is typically called *rotor*, whereas the static part is called *stator*. The latter is physically separated from the rotor and can incorporate the actuator element.

The peculiarity of MEMS mirrors with respect to other kind of devices is that they need to support rotational movement and not a translational movement like most of MEMS. This is needed because most of micromirror applications require a controllable angular scanning of a light source, so that it can be pointed in different positions. The first consequence of this requirement is that micromirrors need to have enough room around them to allow their movement. For example, if we consider a 1 mm diameter mirror rotating by 10°, its edges will travel outwards the rest plane by more than 170 μm. This large movement requires, for example, that a deep enough cavity is realized on the back of the mirror so that no mechanical obstruction is present to the mirror movement. A second consequence of this rotational movement is that all the silicon flexures must be designed to work efficiently under torsion, so that the required scanning frequencies are achieved, and no excessive mechanical stress is built up in the flexure itself. In these regards, the most simple and efficient solution is the straight bar flexure, which can work quite efficiently in torsion and that can be made sufficiently unstressed by making it longer.

The first distinction we must do when talking about micromirrors is about how many scanning directions they can support: typically, micromirrors can rotate around one axis (*monoaxial* micromirror, Fig. 18.4a) or around two axes (*biaxial* micromirror, Fig. 18.4b). There is also some literature about what could be called triaxial micromirrors, adding a third movement to the mechanical structure which is not anyway a rotation (because the third orthogonal rotation would be useless for projection purposes), but an out-of-plane translation (tip-tilt-piston micromirrors) [8] useful for phase control, or a mirror deformation, like a controllable curvature of the mirror for focus or aberration correction of the optical system [9]. Considering anyway their specific interest only in academic research, we will not treat them further in this dissertation.

The easiest monoaxial design can be achieved by attaching to the mirror body a couple of torsional flexures, as reported in Fig. 18.4a. Considering the specific kind of actuation principle pursued, a suitable actuator will be then attached to the mirror body with the purpose of forcing the mirror body into motion.
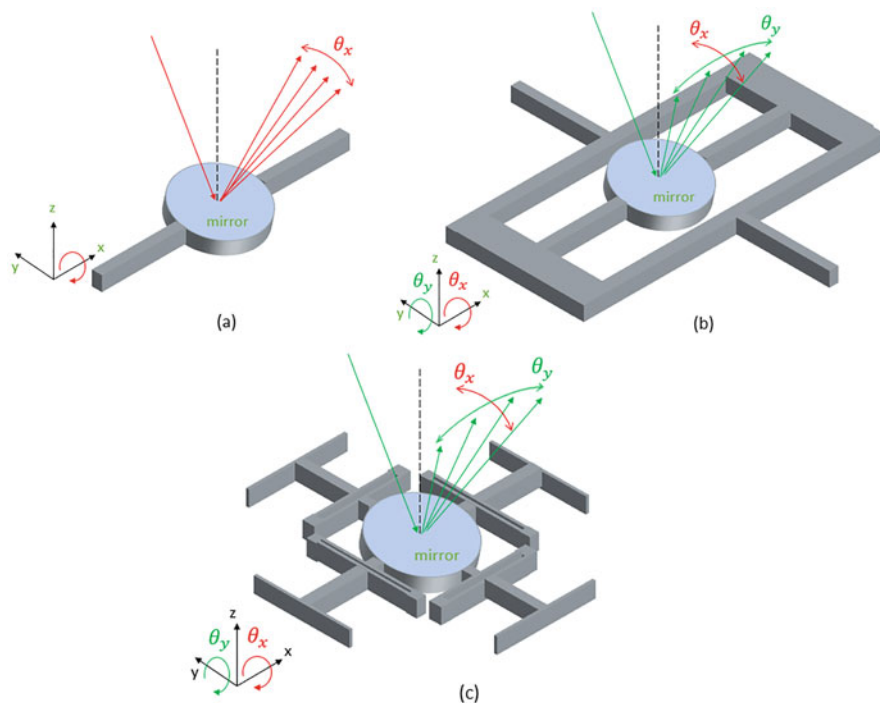
Fig. 18.4 Types of micromirrors: (**a**) monoaxial, (**b**) gimbal biaxial, (**c**) gimbal-less biaxial

On the opposite, a biaxial design needs to sustain rotation of the mirror body around two orthogonal axes. In order to reach this result, two main design solutions are typically used:

- The gimbal design (reported in Fig. 18.4b) is based on the addition of a decoupling rigid frame at which the mirror body and a first couple of torsional flexures are connected, so that rotation is possible around this first axis relative to the frame itself. Such frame is then connected to the fixed substrate by a second set of torsional flexures which allows rotation along a second orthogonal axis. This is the typical design choice for a biaxial micromirror solution, and it is particularly suitable for scanning solutions which require two different and distant scanning frequencies for the two axis, due to the very different inertia of the mirror and frame bodies.
- The gimbal-less design (reported in Fig. 18.4c) avoids instead the presence of a decoupling frame element and it is based on the design of a set of silicon hinges able to support the rotation along the two orthogonal axes. This kind of design solution is more complex due to the plurality of mechanical elements which must work in cooperation, but it is well suited when scanning with similar or equal frequency is needed.
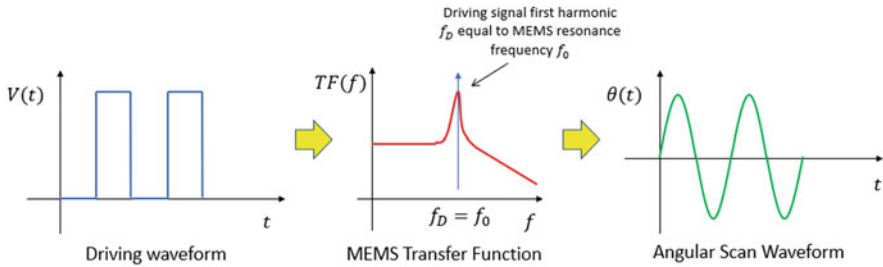
Fig. 18.5 Resonant operation

Most applications require a biaxial scanning to support their scanning requirements (let's consider for example the laser beam scanning projection previously described), so biaxial micromirrors would seem the best choice in most cases. A biaxial scanning can anyway be supported also relying on two monoaxial micromirrors in cascade, and in practice, this solution is preferred in many cases, thanks to its better performances, which comes from the better design optimization achievable for single axis MEMS, whereas biaxial design needs particular care for the additional design trade-offs coming from the integration of two axes scanning into the same MEMS structure.

An additional distinction in micromirrors is the one related to the mode of operation that they need to support. The modes of operation are related to the angular scanning frequency and waveform which are required by the target application:

- *Resonant* operation is a mode of operation in which the micromirror is driven at the frequency of its natural rotational vibration mode, as represented in Fig. 18.5. In this condition, the mechanical structure itself responds with an amplified movement thanks to a mechanical resonance, and larger scanning angles can be achieved with less input electrical power. This kind of operation can anyway only support sinusoidal waveform scanning, because the resonance itself acts as a narrow-band filter. As narrower the resonance is, as larger is the displacement amplification factor. The figure of merit of the resonance is the Q-factor, which represents such amplification factor. To properly work, a resonant micromirror must be designed to have its mechanical eigenfrequency, comprising its manufacturing tolerances, within an acceptable frequency range.

- *Quasi-static* operation is instead a mode of operation where the micromirror can be driven with an arbitrary waveform (see Fig. 18.6), taking into consideration anyway that the micromirror mechanical response will have a bandwidth determined from where its torsional eigenfrequency is located. In such regard, typical quasi-static micromirrors are operated at few tens of hertzs (e.g. 60 Hz), well below their resonance frequencies, which are typically in the range 500 Hz–800 Hz. This mode of operation enables, for example, constant velocity scanning (also called linear scanning) and static operation, that is, angular displacement
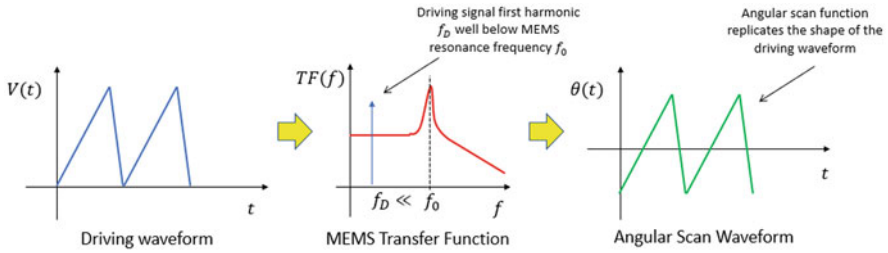
Fig. 18.6 Quasi-static operation

under a DC bias. Quasi-static micromirrors are typically indispensable in most applications thanks to the possibility of handling low frequency and linear scanning required to reach good projection quality without image artefacts.

Finally, micromirrors can be divided based on the wavelength of light radiation they have to reflect. Two main families are typically considered:

- Micromirrors for visible projection must project light in the visible range, typically a triplet of red, green and blue (RGB) laser spots. In this case, the mirror material typically used is aluminium, thanks to its flat reflectance bandwidth of about 90%.
- Micromirrors for infrared projection must project light in the near infrared (NIR) range. In this case, gold is the preferred material to realize the mirror because of its high natural reflectance of about 97%.

18.3   Actuation Principles

Actuators like micromirrors are very much determined by the type of actuation principle exploited to obtain the required motion. Being each actuation principle based on very different physical effects to allow the required electromechanical force conversion, the design principles can vary significantly in the different cases.

In the following, three main actuation principles will be described in detail, which are the most widely adopted in the literature and in the industry. The advantages and disadvantages of these three principles will then be analysed and compared.

18.3.1   Capacitive Actuation and Sensing

Capacitive actuation is likely the first kind of actuation principle adopted for micromirror devices, because of its relative simplicity and inexpensiveness which comes from the fact that the actuator can be realized with the same manufacturing
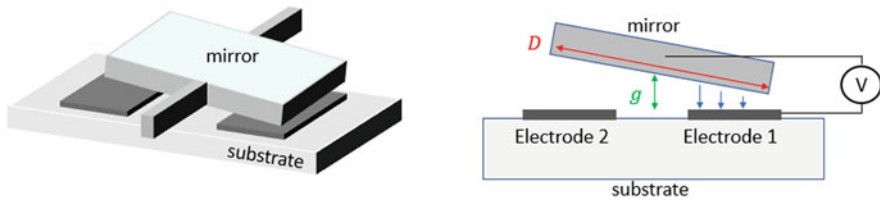
Fig. 18.7 Parallel plate micromirror

process steps which are commonly used to realize other kind of MEMS, for example inertial sensors.

Capacitive actuation is based on the electrostatic force, which is the force built up between the two faces of a capacitor when a potential difference is applied at its two terminals. Electrostatic force arises from the attraction between the electric charges of different sign which accumulate on the faces of the capacitor when it is charged. As a result, the outcome force is always attractive, fact which needs to be taken appropriately into account in order to reach the required actuator operation.

Two main capacitive actuator architectures are typically used.

The first one is the parallel plate architecture: the two faces of the capacitor are realized respectively by the bottom surface of the moving mechanical structure and by a counter-electrode realized on the MEMS substrate. To realize a bidirectional steering of the structure, two separated electrodes are needed, placed to face opposing sides of mechanical structure with respect to its rotational axis. The typical configuration is reported in Fig. 18.7.

The advantage of this architecture is that it can support both resonant and quasi-static operation without additional manufacturing complexity. Its biggest drawback is that the gap between the moving structure and the driving electrodes limits the maximum steering angle both mechanically than electrostatically. The mechanical limitation is trivial to understand referring to Fig. 18.7. Because of the tilting motion of the mechanical structure, its edges will touch the substrate and the driving electrodes when the critical angle θ_{crit} is reached, related to the geometrical dimensions of the MEMS in the following way:

$$\theta_{crit} = \text{atan}\left(\frac{2g}{D}\right) \qquad (18.1)$$

where g is the gap between moving structure and driving electrodes and D is the micromirror width, typically equal to its reflecting area diameter.

In addition, pull-in effects could further limit the maximum achievable working angle. Pull-in is an effect for which the mechanical structure collapses over the driving electrode because the position-dependent component of the electrostatic force cancels out the restoring force of the torsional spring. For this kind of MEMS, anyway it has been demonstrated that pull-in voltage can be pushed to be larger
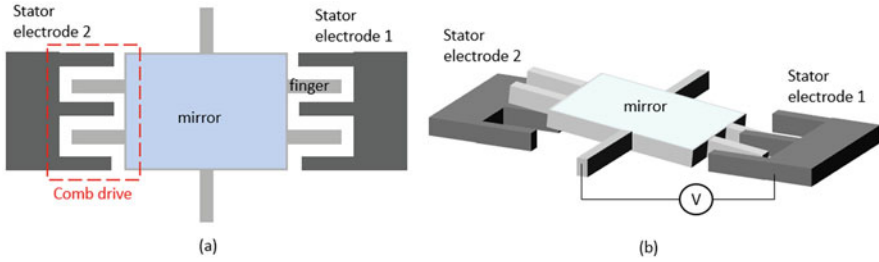
Fig. 18.8   Planar comb drive: (**a**) top view, (**b**) lateral view

than the voltage needed to reach the critical angle θ_{crit} [10], making the mechanical constraint the only limitation to the maximum achievable angle.

Using Eq. 18.1, it can be estimated that for a typical mirror diameter of 1 mm, a gap of about 9 µm would be needed to reach a tilting angle of 1 degree. Such gap dimensions could become technologically complex to realize so that only limited opening angles are achievable, impractical for most applications.

Nevertheless, this actuation scheme has found wide adoption mainly in array micromirrors [11], where the single mirror dimension (few micron large) is no more a limiting factor for the mechanical angle and where the fact that the actuator is hidden below the mirror itself has been found highly advantageous to increase the mirror fill factor.

The second architecture for capacitive actuators is the comb drive. A comb drive is composed by a set of closely packed cantilevers (called fingers) attached to the rotor structure and interdigitated to a specular set of cantilevers attached to a fixed structure, that is, the stator (Fig. 18.8). The capacitor is then obtained by the facing lateral surfaces of the fingers and can be easily increased by adding more fingers to the actuator or by changing their geometrical dimensions.

This architecture is very attractive thanks to its integration simplicity because it can be realized with the same process step used to pattern the mechanical structure. Its main limitation is related to the fact that, being the moving comb fingers and the fixed ones realized in the same plane, the attraction force at rest condition is almost null, so they cannot be used for quasi-static actuation. Resonant operation is anyway feasible thanks to small force imbalances from manufacturing non-idealities, which are able to put in motion the MEMS.

Therefore, a more complex structure is required to obtain quasi-static operation in which an out-of-plane offset is provided by construction between moving fingers and fixed fingers (see Fig. 18.9) and tight alignment between the two layers patterns are needed to keep similar performances to the in-plane comb fingers. Such solution is called staggered comb fingers actuator.

As a first step, let's focus on in-plane comb fingers case and let's derive the electrostatic torque T_{el} relation to the voltage V. Let us start considering the electrostatic energy U in the comb capacitor, which will assume the form:
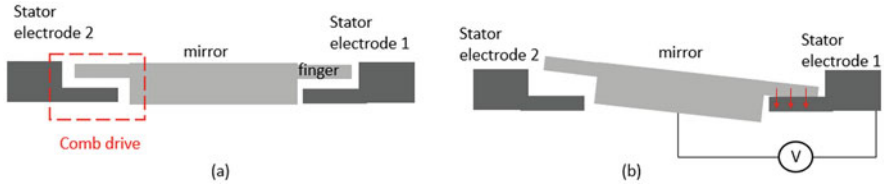
Fig. 18.9 Staggered comb fingers cross section: (**a**) in rest position, (**b**) tilted position under bias
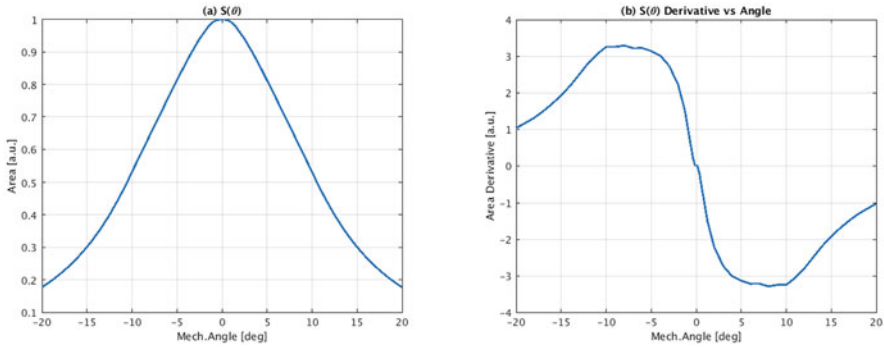

Fig. 18.10 Facing area versus tilt angle (a) and its derivative (b)

$$U = \frac{1}{2} C\left(\theta\right) V^2 \tag{18.2}$$

where $C(\theta)$ is the comb capacitance, which is a function of the moving structure tilting angle θ due to the changing facing area of the electrodes during tilt.

The capacitance relation to the comb fingers geometrical dimensions can be then reported as

$$C\left(\theta\right) = 2N_f \frac{S\left(\theta\right)}{g} \tag{18.3}$$

where N_f is the number of comb fingers, g is the gap between the comb fingers and $S(\theta)$ is a function which represents the comb finger facing area value versus the rotor tilting angle. The function $S(\theta)$ cannot be analytically determined but it can be estimated, for example, through Finite Element Modelling (FEM). An example of $S(\theta)$ function and its derivative are reported in Fig. 18.10.

The electrostatic torque can be obtained then by differentiating Eq. 18.2 with respect to the tilting angle:

$$T_{el} = \frac{\partial U}{\partial \theta} = N_f \frac{1}{g} \frac{\partial S\left(\theta\right)}{\partial \theta} V^2 \tag{18.4}$$

It can be observed that the electrostatic torque is directly proportional to the number of fingers and to the square of the driving voltage and inversely proportional to the gap between fingers. It is also to be noted that the torque depends on the derivative of the single finger facing surface with respect to tilting angle.

The same exact considerations can be done for the staggered comb fingers case obtaining the same result reported in Eq. 18.4 except for the fact that the function $\partial S(\theta)/\partial\theta$ will be different due to the different comb finger geometry. We will indicate the facing area derivative function for the staggered comb drive with $\partial S^{'}(\theta)/\partial\theta$.

From a practical standpoint, the easiest implementation of a staggered comb drive requires two structural levels in which the comb fingers are patterned and with an offset equal to the full thickness of one layer. This translates into the fact that the derivative function for the staggered comb is practically equivalent in shape to the in-plane derivative function with an angular offset θ_{off}:

$$\frac{\partial S'(\theta)}{\partial\theta} \cong \frac{\partial S\left(\theta - \theta_{off}\right)}{\partial\theta} \tag{18.5}$$

It can be seen from Fig. 18.10 that the obtained electrostatic torque is linear only on a small angular portion, meaning that a linearization is needed through driving waveform shaping if a linear scan is required.

In addition, being the electrostatic force only attractive, two comb fingers set with opposite out-of-plane offset are needed to provide a scanning in both angular directions.

In both cases, to have torques large enough to reach the typical required opening angle in the range of 7°–10°, a driving voltage between 100 V and 200 V is needed.

Most micromirror applications require strict projected spot position accuracy which are not possible to be achieved by open loop driving due to effects like self-resonance excitation in quasi-static scanners or change of frequency due to temperature in resonant scanners.

To allow tighter position accuracies by closed loop control, a measurement of the tilt position of the scanner is needed. Also in this case, capacitive effects come to help by a position measurement method based on the same comb fingers used for actuation, without added complexity to the MEMS process.

As a matter of fact, let us consider a comb drive biased at a constant voltage V_{sense}: due to the tilting movement, the capacitance will change in time. As a result, a current I_{sense} will be generated at the ends of the capacitor given by:

$$I_{sense} = \frac{dQ}{dt} = \frac{d\left(C\left(\theta(t)\right)V_{sense}\right)}{dt} = N_f \frac{1}{g}\frac{\partial S\left(\theta(t)\right)}{\partial\theta}\frac{d\theta}{dt}V_{sense} \tag{18.6}$$

Such current is proportional to the velocity of the mirror, so also relevant information on the position can be extrapolated. The presence of the derivative function $\partial S(\theta)/\partial\theta$ in the relation breaks down anyway the linearity of the relation so
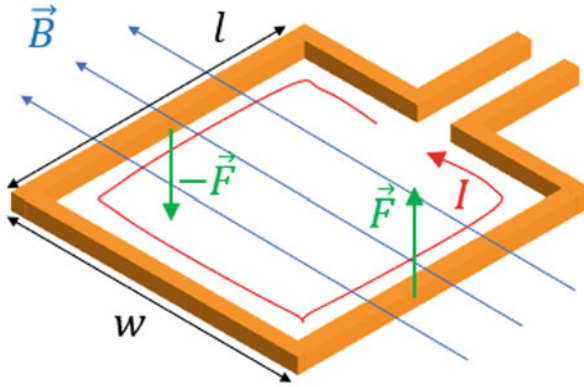
Fig. 18.11 Lorentz's force on a wire loop

that additional considerations will be needed to design an effective control, which anyway will not be treated here.

18.3.2 Magnetic Actuation

An alternative actuation solution to electrostatic force, which has been widely investigated, is magnetic actuation.

Magnetic actuation exploits Lorentz's force to create an electrically controllable torque to drive the MEMS. Lorentz's force is the force created on a wire of length L immersed in an external magnetic field $\overrightarrow{B}$ in which it is flowing a current I:

$$\overrightarrow{F}_L = IL\,\hat{t} \times \overrightarrow{B}$$

where $\hat{t}$ represents the versor directed along the wire.

As we can see, Lorentz's force depends on the vector product between the current carrying wire direction and the external magnetic field. As a result, a wire directed along the magnetic field will not suffer any force, whereas a wire directed perpendicularly to the magnetic field will be subject to the maximum force value.

Let's now consider a wire loop as the one reported in Fig. 18.11. As per what we have described before, the two wire portions directed along the field will not provide any force, whereas the other two wire portions perpendicular to the field will be subject to a force equal in modulus but opposite in direction, that is, a force couple.

The torqueing moment T_L associated to this force couple is

$$T_L = BILw = BIS$$

where w is the width of the wire loop, so the moment is proportional to the area of the wire loop. This relation between moment and loop area has been demonstrated for a rectangular wire loop, but it is valid in general for each loop shape.

In the case we are dealing with a coil composed by N_c wire loops, the torqueing moment of each wire loop will sum up to the others and the total coil moment will become

$$T_{coil} = N_c B I S = K_t I$$

where we have defined a motor constant $K_t \doteq N_c BS$, similarly to what typically done for electric motors. It is easy to understand that, in case the magnetic field B is not homogeneous and dependent from the MEMS angular position θ, as in most of the practical applications, the motor constant will not be a constant anymore and will assume a more general definition

$$K_t(\theta) \doteq \oint \vec{r} \times d\vec{F_L} = \oint \vec{r} \times \left(d\vec{l} \times \vec{B} \right)$$

where $\vec{r}$ is the vector distance from the rotation axis and $d\vec{l}$ is a vector having the local direction of the coil wire and a modulus equal to an infinitesimal length of the wire itself.

The motor constant K_t describes then all the intrinsic properties of the actuator related to its geometry and the magnetic field in which it is moving.

Then Lorentz's force provides an effective way to have a torque controllable through the electrical current flowing into the wire. Differently from the electrostatic case, the torque is linearly dependent from the current, so a bidirectional driving is possible because the actuation forces can be attractive or repulsive. This is particularly helpful for quasi-static micromirrors because a bidirectional scanning is achievable without the need to duplicate the actuator as in the electrostatic case.

We can then exploit the Lorentz's force for actuating a MEMS mirror just by integrating a coil onto the moving mass and enclosing it between permanent magnets which can provide inexpensively a large magnetic field. This is the so-called *moving-coil* architecture (Fig. 18.12a).

It exists also a converse architecture, the so-called *moving-magnet* design, which is based on having magnetic material deposited over the MEMS moving structure and on moving them through the magnetic field generated by the current flowing into an external coil or electromagnet [12]. This architecture is anyway providing an intrinsically weaker actuation torque due to many reasons (e.g. small magnet volume translates into small magnetic fields, not mature MEMS permanent magnet material integration technologies, very small magnetic field generated by external coil). Therefore, we will focus our attention only on the moving-coil architecture.

As we have seen previously, the physical quantity providing the actuation force is the electric current flowing into the coil. Being the coil a resistive load for the driving generator, a direct average power dissipation P_{diss} is present on the MEMS given by the Joule effect:
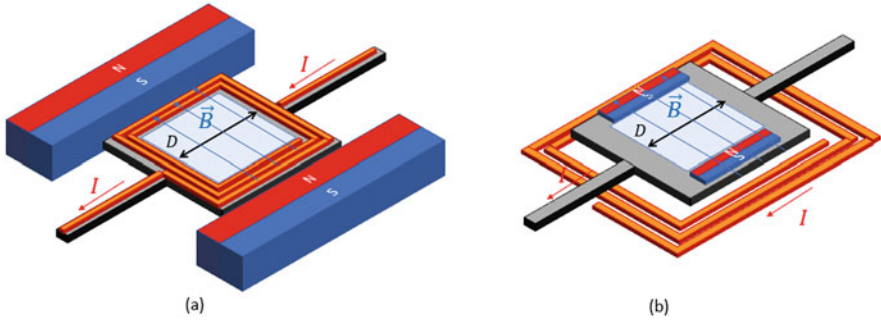
Fig. 18.12 Magnetic mirror architectures: (a) moving coil, (b) moving magnet

$$P_{diss} = R_{coil} I_{rms}^2$$

where R_{coil} is representing the resistance value of the coil and I_{rms} the RMS value of the driving current.

As a result, in a magnetically actuated micromirror, it is critical to minimize both the coil resistance and the driving current RMS value, otherwise a significant power dissipation up to some hundreds of milliwatts could be easily reached. A large power dissipation would be detrimental not only for the final application, where such power losses are very unattractive for battery-based devices, but also for the device reliability when high temperatures could be reached locally due to self-heating coming from the transformation of electric power into heat by the Joule effect.

To minimize coil resistance, the preferred approach is choosing a material with very low resistivity and to optimize coil wire parameters (thickness, width, pitch, number of windings) in order to have the maximum actuation torque for the minimum power consumption. In such regards, it is important to consider that the self-heating effect previously described will contribute to increase the load resistance since most conductors show an increase of resistivity with temperature T, following the law:

$$R(T) = R(T_0)(1 + \alpha_T (T - T_0))$$

Here T_0 is representing the reference temperature and α_T is the coefficient of thermal variation of resistivity in temperature.

As a result, metals are preferred with respect to silicon for manufacturing the integrated coils, and in detail, copper is the material of choice for these devices, thanks to its demonstrated integration capability into MEMS processes and its high conductivity.

Instead, to minimize the driving current keeping the torque level unchanged, the typical approach is maximizing the external magnetic field provided by the permanent magnets. This can be achieved first by an appropriate choice of permanent

magnets material. In such regard, the solution of choice are the neodymium–iron–boron magnets, which are inexpensive, and which have proven to provide among the largest magnetic fields achievable among permanent magnetic materials.

Second, a good magnetic assembly design is required, minimizing the distance between the MEMS coil and magnet itself. In such a way, magnetic field values around 0.2–0.3 T are typically achieved in these applications. The volume of the permanent magnet is anyway typically much larger than that of the MEMS chip and it is not possible to scale it significantly without losing in actuation performance, making it hard to reach very small package form factors.

Considering these magnetic field levels and the low resistor values needed to minimize power consumption, currents up to few hundreds of milliamperes can be sustained. The voltage needed for actuation can then stay below 5 V, allowing the use of standard CMOS electronics technologies for driving.

Magnetic micromirrors also present an additional reliability requirement: we have seen that the driving coil is realized with a metal wire that needs to be patterned over the moving structure. Therefore, a metal connection needs to pass onto the silicon flexures around which the mirror rotates and so it is subject to a cyclic mechanical stress. It is then required to use metal materials which are fatigue resistant, to grant the electrical contact over the whole lifetime of the device.

Magnetic actuation is often used also when biaxial scanning micromirrors are needed. In fact, biaxial actuation is more easily implemented with magnetic mirrors, whereas electrostatic micromirrors would need complex processes with vertical electrical insulation to be realized over the moving structure [13].

On the opposite, in magnetically actuated mirrors, it is possible to design two different driving coils, one for each axis, with the same metal layers. One coil will couple with the rotation along a first axis, another one will couple with the rotation along a second perpendicular axis (see Fig. 18.13). A diagonal magnetic field will be required to provide an effective Lorentz's force along both axes.

This design is anyway quite complex to handle: two separate coils need to be designed requiring additional space; additional metal layers are passing over stressed flexure increasing risks of metal trace fatigue.

A more compact and elegant solution have been identified in [14], where a single coil is patterned onto the frame of a gimbal structure. In the coil, two different driving current waveforms are summed up and injected at the same moment. The mechanical structure will then act as a mechanical filter and each axis will react respectively to only one of these frequencies.

In order for this solution to properly work, the two driving frequencies need to be well separated in order to reduce as much as possible cross-axis actuation. This typically translates into having a first axis with a resonant frequency below 1 kHz and a second axis with resonant frequency higher than 20 kHz.
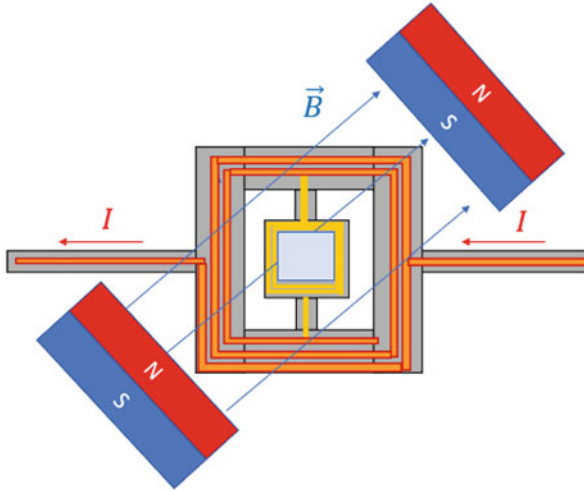
Fig. 18.13 Double coil magnetic mirror

18.3.3 Thin-Film Piezoelectric Actuation

Recently, the emerging of mature industrial processes for thin-film piezoelectric layers integration into MEMS technologies has generated lots of opportunities for the exploration of piezoelectric actuation into MEMS, including micromirrors.

Piezoelectric actuation is attractive thanks to the possibility of integrating a fully working actuator directly on the MEMS chip, which allows complete electromechanical wafer level testing, differently from magnetic micromirrors where the need of external permanent magnets make possible to measure the actuation characteristics only on the final assembled component, shifting potential yield losses later into the production chain and increasing production cost.

In addition, this kind of actuation exploits a physical effect allowing larger actuation forces than electrostatic-based solution enabling better scanner characteristics (larger scanning angle, larger diameter etc.).

Micromirror actuators make use of the converse piezoelectric effect, which consists of the fact that a piezoelectric material shows a change of its mechanical dimensions when subject to an external electric field (see Fig. 18.14b).

In the typical MEMS application, a thin-film piezoelectric material is deposited over a silicon substrate and patterned onto a mechanical structure. Upon voltage biasing, the piezoelectric material would like to change its dimensions, but it cannot do it freely because constrained by the silicon structure so that it builds up internal stresses. As a result, a mechanical force is transferred to the mechanical structure which is consequently deformed.

Among the piezoelectric materials, the most widely used for actuation purposes is the lead zirconate titanate, typically known as PZT, thanks to its demonstrated
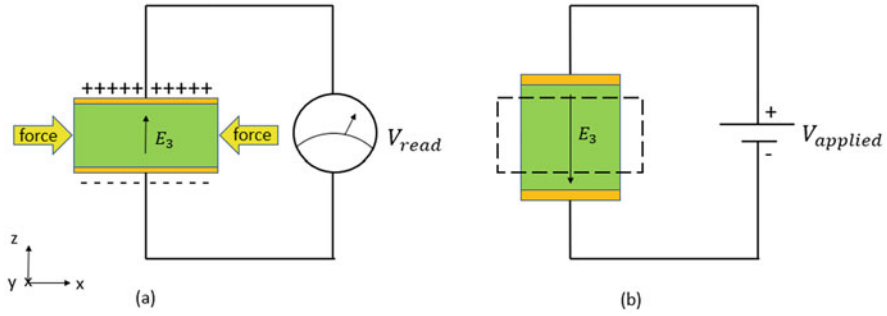
Fig. 18.14 Piezoelectric effect: (**a**) direct, (**b**) converse
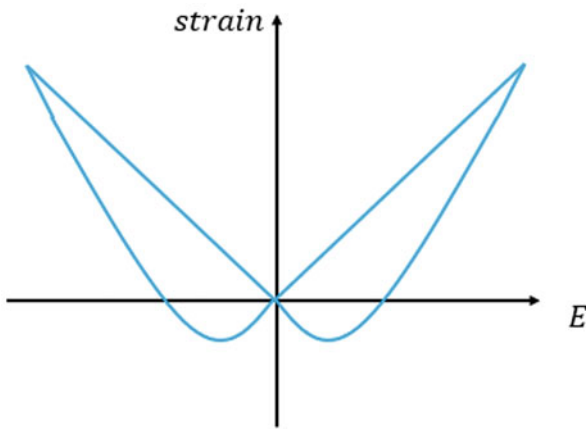

Fig. 18.15 Typical strain versus voltage characteristics of thin-film PZT material

integration capability into MEMS processes and its large piezoelectric parameters compared to other thin-film piezoelectric material.

The piezoelectric constitutive equations, which have been reported in Chap. 10, would lead readers to think that the piezoelectric effect is linearly dependent from the electric field and that a perfect actuation force reversal would be possible upon reversal of the electric field.

This is generally not true for PZT and in particular for its thin films because of its ferroelectric and electrostrictive nature. In fact, in PZT thin films, operating electric fields do easily exceed the coercive field of the material and the material piezoelectric response assumes significant nonlinear fashion, as reported in Fig. 18.15. In particular, PZT shows deformation in the same direction upon complete reversal of the electric field direction, making it unpractical to work with bipolar bias.

It must also be noted that bipolar cycling of the PZT is not suggested in standard operation due to fast insurgence of ferroelectric and piezoelectric fatigue of the
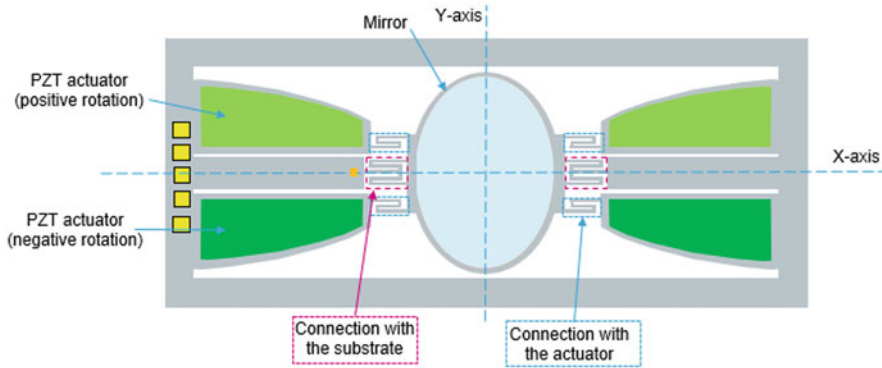
Fig. 18.16 Exemplificative scheme of piezoelectric scanner design

material [15], which causes a degradation of the piezoelectric properties and so of the actuator itself.

Consequently, PZT-based micromirrors need to work in unipolar biasing conditions and rely on an actuation force which has always the same direction. In this regard, PZT-based micromirrors are subject to similar design considerations as the electrostatic micromirrors which must rely only on attractive force. It is also noted that staying in unipolar regime, a linearized model of the piezoelectric force is typically sufficiently accurate to keep using the constitutive equations in Chap. 10 without needing to develop more complex, nonlinear models.

Generating a torsional movement with a piezoelectric actuator, naturally providing an out-of-plane translation movement, is not a trivial task. The working principle of one of the most efficient design solutions [16] will be described in the following, exemplificative of the typical micromirror scanner design.

The piezoelectric micromirror structure comprises a couple of torsional flexures connected to the mirror body on one side and at the fixed substrate on the other side. Two sets of cantilevers with piezoelectric patches on top extend then from the fixed frame up to the edges of the mirror body and connects to it through folded springs, which have the task of efficiently transferring the out-of-plane force to the mirror and allowing the mirror body rotation at the same time. This structure is illustrated in Fig. 18.16. Such sets are put on opposite sides with respect to the rotation axis so that their alternate actuation can create opposite rotation directions of the mirror body. Appropriate tuning of the dimensional characteristics of the structure allows then to support quasi-static actuation or resonant actuation.

An analytic description of a piezoelectric micromirror would be very complex and very much related to the specific design of interest due to the complicated interplay between different materials and multiple mechanical elements. As a result, FEM is considered an essential tool for the design of piezoelectric based micromirrors.

Anyway, meaningful physical insight can be gained by relying on appropriate lumped equivalent models, where an equivalence between mechanical elements and electrical components is drawn [17].

In particular, the electromechanical transformation factor η can be defined as

$$\eta = \frac{dQ}{d\theta}$$

where Q is the charge accumulated on the capacitor and θ the mirror tilt angle. Such electromechanical transformation factor can be found by FEM and used also to have an estimate of the effective piezoelectric torque T_{pze} by using the following equivalence relation:

$$T_{pze} = \eta V$$

The input actuation torque is then dependent only from the driving voltage and the electromechanical transformation factor.

It can be demonstrated [17] that such transformation factor is proportional to the d_{31} piezoelectric coefficient introduced in Chap. 10 and dependent on the stress in the piezoelectric material induced by a rotation by an angle θ, so a piezoelectric actuator is more efficient not only if its piezoelectric properties are better but also if it is stressed sufficiently by the target displacement, which determines the need of appropriate design optimization of the mechanical structure.

18.3.4 Comparison Between Actuation Principles

Now that we have seen the basic properties of the main actuation technologies for micromirrors, let's compare their benefits and the limitations.

The summary of the comparison is reported in Table 18.1:

In terms of pure maximum mechanical torque achievable, electromagnetic and piezoelectric actuations are able to provide larger forces, whereas electrostatic force is limited by the intrinsic weakness of electrostatic attraction and by the maximum

Table 18.1 Comparison of the actuation technologies

	Electrostatic	Electromagnetic	Piezoelectric
Mechanical torque	Low (< 1uNm)	High (>1uNm)	High (>1uNm)
Force direction	Monodirectional	Bidirectional	Monodirectional
Electromechanical efficiency	High	Mid	High
Driving voltage	$\leq$ 200 V	$\leq$ 5 V	$\leq$ 50 V
Power consumption	Low	High	Low
Volume occupation	Mid	Large	Small

driving voltage safely achievable. As a result, electromagnetic and piezoelectric actuations can achieve better scan performances.

To provide good performances, electrostatic actuation needs also large driving voltages, up to 200 V, whereas piezoelectric actuation based on PZT can work with voltages below 50 V and electromagnetic mirrors can stay below 5 V if very small coil resistances are achieved.

Electromagnetic solution has then an intrinsically linear force, which simplifies the design especially when dealing with quasi-static actuation, but on the other side, it is affected by a low-actuation efficiency since a direct power dissipation is happening on the MEMS coil due to Joule effect. Instead, electrostatic and piezoelectric actuations are both having a capacitive drive load which is intrinsically less subject to power dissipation.

In terms of final scanning module size, magnetic solution requires large room to accommodate the permanent magnets needed to create the actuation forces, whereas both electrostatic and piezoelectric solutions can integrate their actuator directly at MEMS process level. In terms of size, then, piezoelectric actuation has an additional advantage related to its intrinsically higher force, so that smaller actuators can be designed with respect to the electrostatic case.

Therefore, electrostatic is a good solution when limited scan performances are sufficient thanks to its efficiency and small dimensions, at the cost of a higher driving electronics complexity required to generate the high voltage driving signals.

Electromagnetic actuation is a good solution when large scan performances or very large mirrors are required at the expense of module size and power consumption.

Finally, piezoelectric actuation offers good compromises in terms of actuation force, size and power consumptions which make this technology very appealing for the commercial application at the price of a higher design complexity.

18.4   Technology Platform

In this section, the technology architectures to realize a Raster scanning mirror are shown and discussed. The technology platform is strictly related to the actuation principle, to packaging constraint and reliability target.

18.4.1   Comb Finger Structure Realization for Capacitive micromirror

In this subsection it is analysed the technology to realize a capacitive micromirror with parallel comb finger. Such technology must integrate a mobile mass, a reflective
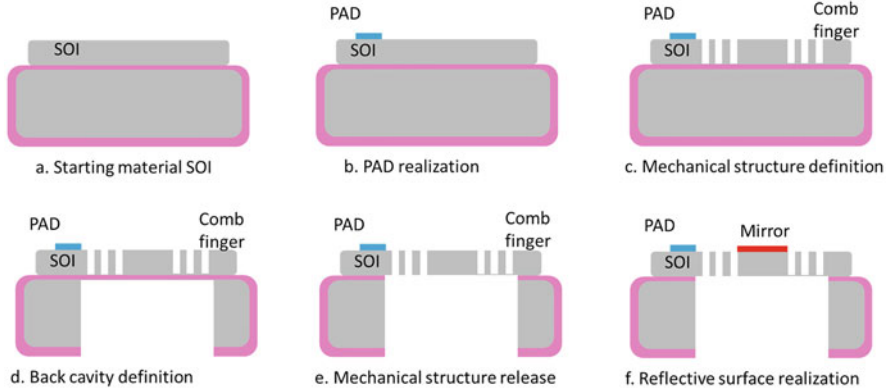
Fig. 18.17 schematic process flow for Electrostatically actuated Resonant Mirror: (**a**) starting material, (**b**) pad realization, (**c**) mechanical structure definition, (**d**) back cavity definition, (**e**) mechanical structure release, (**f**) reflective surface realization

surface and a comb finger array that works as actuator and as sensing structure for the mirror position.

A wide part of the published literature is on electrostatic MEMS mirrors, since their fabrication requires the availability of few technology steps, as it will explained in this section.

The simplest process architecture is the one that realizes a resonant, mono-axial, electrostatic mirror. The process schematic is the one explained in [18] and summarized in Fig. 18.17. An SOI wafer is chosen as starting material (for applications with 720p resolution, a 40-60 μm is a suitable SOI thickness), with a low resistivity (1–15 mOhm cm). A first metal layer is deposited on silicon and patterned through photolithography and etch, to realize the pads (Fig. 18.17b). The composition of the metal and its stack depends on the constraint relative to wire bonding and on the desired ohmic characteristic of the contact. After the Pad definition, the mirror mechanical structure is realized through photolithography and dry silicon etch (Fig. 18.17c). During this step, the in-plane comb fingers, the torsional flexure, the electrical domain (stator and rotor) and the mirror area are defined by removing the silicon of the SOI layer and by landing on buried oxide. After these operations, the wafer is reversed and, by using a front to back aligner, the back-cavity mask is realized and the following dry silicon etch helps to remove the silicon under the mirror, stopping on buried oxide again (Fig. 18.17d). The mechanical structure complete release is obtained through hydrofluoric acid (HF) etch of the buried oxide (Fig. 18.17e). The reflective surface is realized through proper metal deposition by using shadow mask technique (Fig. 18.17f).

This simple process scheme has one drawback if it must be manufactured in high volume: during the wafer reverse, the front of the wafer can be damaged by the handling of the equipment and a sort of front protection (sticky tape, temporary
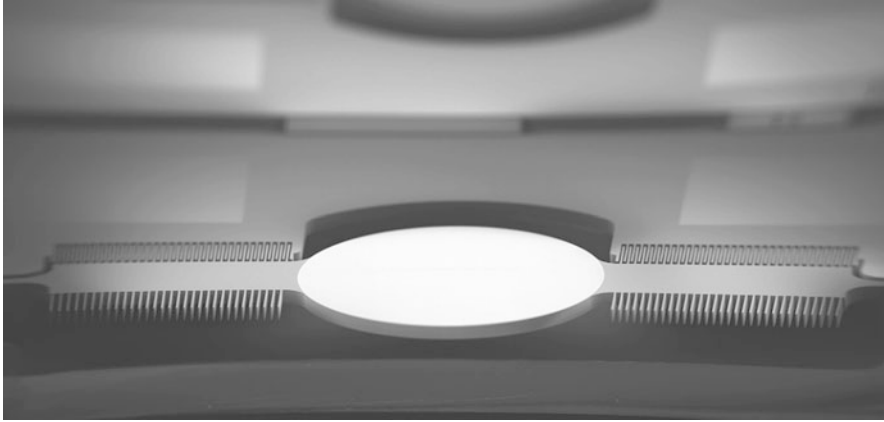
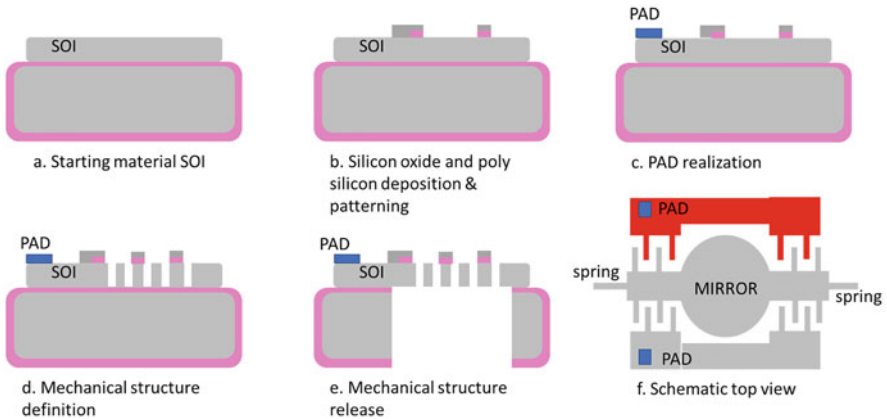**Fig. 18.18** SEM picture of electrostatic resonant mirror

Fig. 18.19 Schematic process flow for electrostatically actuated resonant mirror with deterministic oscillation start: (**a**) starting material, (**b**) silicon oxide and polysilicon deposition and patterning, (**c**) pad realization, (**d**) mechanical structure definition, (**e**) mechanical structure release, (**f**) final device schematic top view

bonding and polymeric film) is necessary. In Fig. 18.18, an example of finished resonant micromirror is shown.

Even if the structure looks perfectly symmetric and the force fully balanced, small asymmetry due to wafer processing allows the start of oscillation. To have a deterministic oscillation start, that is mandatory in pico-projection application, an asymmetry in wafer process can be created in the structure as described in Fig. 18.19. Starting from previously described process flow, a Silicon dioxide and polysilicon deposition is performed before pad realization. Each layer deposition is followed by a patterning step, to short-circuit the polysilicon structure to the SOI (as shown in Fig. 18.19b). Thanks to the presence of Silicon dioxide, the etch of

polysilicon does not damage the starting SOI surface. As shown in Fig. 18.19d, this small capacitor is added on stator fingers in asymmetric layout, to create an asymmetry in the electric field. A schematic device top view is reported in Fig. 18.19f, where in red, it is highlighted the region where the polysilicon is left on the top of stator finger. A simpler process approach is to realize a local thinning of stator finger, by using a silicon dry etch at fixed time.

The process scheme for the realization of the electrostatic quasi-static micromirror is slightly more complex since a staggered comb finger structure is needed.

To realize the staggered structure, a double structural layer (double SOI, or SOI and Epi-poly) is necessary, and the comb fingers will be defined in both structural layers. This fact adds a further complexity: in order to avoid the pull-in of the electrodes during mirror operation, the alignment between the staggered fingers must be very tight, or other solution must be adopted on process side. Two different process approaches to realize the staggered solution will be explained.

The first process scheme uses a direct lithographic alignment between the comb fingers. The main process steps are summarized in Fig. 18.20 and the good result on the final device depends on the level of performance of the lithographic alignment in infrared. The starting material is an SOI wafer, where an insulating layer of silicon dioxide is realized by oxidation or deposition. The aim of such dielectric is two-fold: the first is to be the landing layer for the silicon etch, the second is to create a separation between the two electrical domain of the rotor and the stator. In order to realize the electrical connection to the SOI layer, the oxide can be patterned (Fig. 18.20b) or a more complex system of oxide, polysilicon as interconnection and oxide can be realized as explained in [19]. After the realization of the electrical
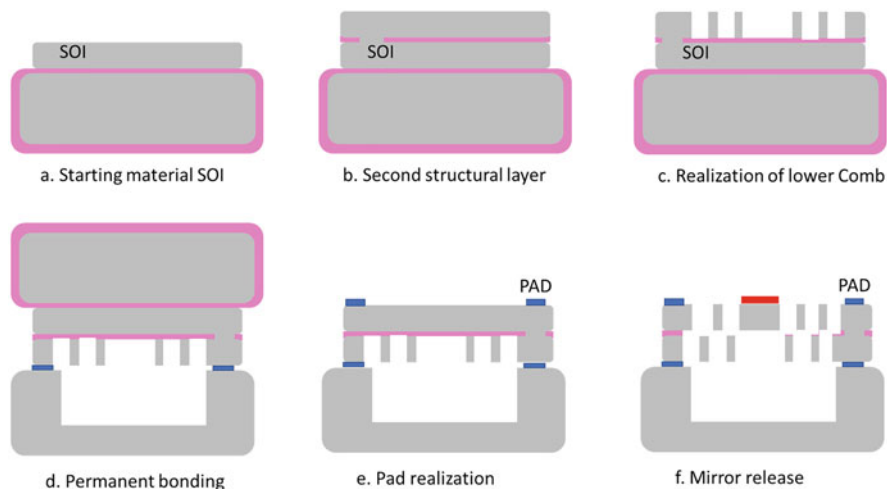

Fig. 18.20 Schematic process flow for electrostatically actuated linear mirror with staggered comb-finger: (**a**) starting material, (**b**) second structural layer deposition, (**c**) realization of lower comb, (**d**) permanent bonding, (**e**) pad realization, (**f**) mirror release
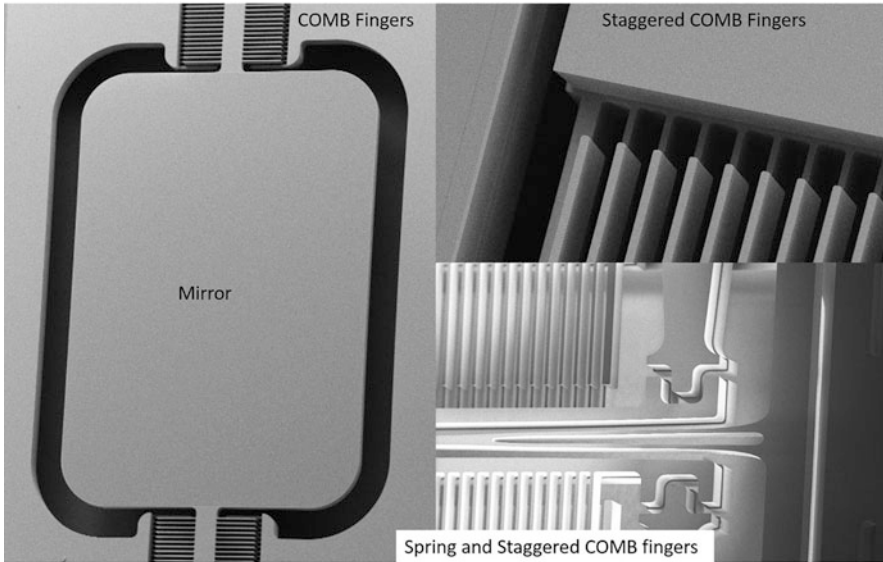
Fig. 18.21 Electrostatic Linear Mirror. Detail of spring and staggered comb fingers

separation of the domain, an Epitaxial silicon layer is grown and through chemical mechanical polishing the same thickness of the starting SOI is reached (for 720p resolution, 40 µm is a suitable thickness). The lower comb fingers array is then realized by using photolithography and dry silicon etch and by stopping on buried oxide (Fig. 18.20c); if it is requested by application, a reinforcement under the mirror structure can be realized with this mask. Such patterned wafer is bonded, through permanent W2W bonding technique to a cavity silicon wafer (Fig. 18.20d). The cavity under the mirror is necessary in order to allow structure movement. The handle layer of the starting SOI material is removed, by using a grinder wheel or chemical solution/gas (Fig. 18.20e). Metal layer for PAD is deposited and patterned (Fig. 18.20e), with similar consideration done on resonant mirror flow. The movable structure definition (mirror structure, upper comb finger and spring) is completed by the photolithography of the last mask and the following dry silicon etch. This mask must be aligned with tight tolerance with respect to the lower comb finger. For a 720p linear mirror that is actuated with 180–200 V bias voltage, the maximum acceptable misalignment between the comb finger is 0.7 µm. The whole structure is released by HF and, at the end, the reflective surface is realized by depositing the metal through a shadow mask (Fig. 18.20f).

In Fig. 18.21, SEM picture of mirror device with staggered comb finger structure, realized with the process scheme described above, is shown.

The second process scheme realized a well control staggered structure by using a self-aligned silicon dry etch between the two comb structures. This solution is cited in [19] and [20].The idea is to define both upper and lower comb fingers with
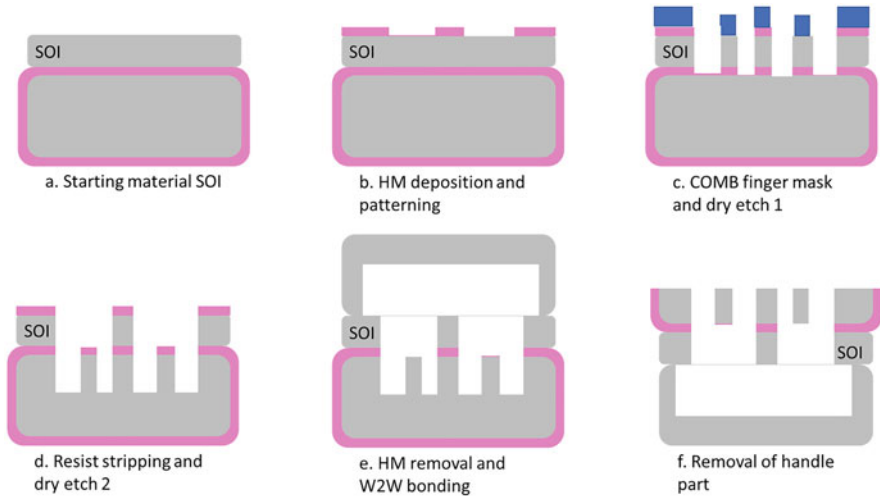
Fig. 18.22 Schematic process flow for Electrostatically actuated linear Mirror with staggered comb-finger (self-aligned approach): (**a**) starting material, (**b**) hard mask (HM) deposition and patterning, (**c**) comb finger mask and first dry etch, (**d**) resist stripping and second dry etch, (**e**) HM removal and W2W bonding, (**f**) removal of handle part

a single dry silicon etch, by using Hard mask and photoresist. A possible flow is the one described in [20] and shown in Fig. 18.22.

The starting material is an SOI wafer, where a Hard Mask (e.g. silicon dioxide layer) is deposited and then selectively removed, in comb finger region (Fig. 18.22b). A photoresist mask is realized to define comb fingers. As shown in Fig. 18.22 c, the photo resist (blue shape) protect both silicon surface and pre-patterned hard mask. After the mask exposure and resist development, a dry etch is performed. The dry etch is composed by three different steps: a first hard mask etch, since the mask is enclosed in previous hard mask patterning, a silicon dry etch, that define the lower comb, and a final buried oxide dry etch. The resist is then removed, and the wafer process continues with a silicon dry etch. During this step (Fig. 18.22d), the upper comb finger is defined using hard mask and buried oxide as silicon etch stop, while the lower fingers, not protected by the hard mask, are etched away. Such wafer is bonded to another one, by using W2W permanent bonding technique, and the process ends by removing the silicon and discovering the upper comb fingers. The simplified process flow here described can be improved by starting from a wafer with two structural layers (SOI and epipoly, or a double epipoly layer), in order to have a better thickness control of the upper comb finger and an etch stop for the last silicon removal step. The other consideration regards the actuation: such approach creates a staggered comb-finger structure slightly different respect to the one described in Fig. 18.22, resulting in a less effective electrostatic force, due to a typically smaller facing area compared to fingers with same thickness.
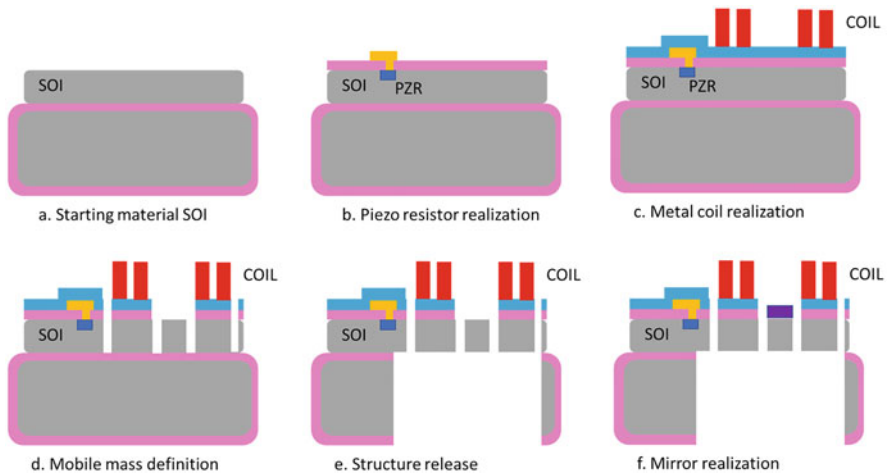
Fig. 18.23 Schematic process flow for Electromagnetic actuated uniaxial Mirror (moving coil approach): (**a**) starting material, (**b**) piezo resistor realization, (**c**) coil metal realization, (**d**) mobile mass definition, (**e**) structure release, (**f**) mirror realization

18.4.2 Electromagnetic micromirror Technology

The electromagnetic mirror technology consists on the realization of a reflective surface, the mobile structure, the metal wire necessary for the application of the Lorentz force and the sensing of the mirror position. The permanent magnet is usually placed at die level, in the MEMS package. This approach is called "moving coil"; there is a second possible configuration that uses a fixed coil and a moving magnet. In this section, it will be explained the technology needed for the realization of the first, while for the second, the suggested publication is [21].

In Fig. 18.23, it is shown the process sequence for the realization of electromagnetic actuated micromirror.

The moving structure is realized using an SOI layer; to reach a 720p resolution a suitable thickness is 40–50 μm. While the sensing in an electrostatically actuated mirror is the comb finger capacitance itself and no dedicated process steps are necessary, in electromagnetic mirror, four piezo resistors connected in Wheatstone bridge configuration have to be realized on silicon to verify the mirror movement during actuation (Fig. 18.23b). A powerful sensitive system can be achieved using implanted diffused resistor. The usage of boron doped starting SOI layer, a good lithographic alignment with silicon crystal direction, and a smart layout allow to reach a high sensitivity value (e.g. 5 mV/V/deg).The realization of piezo-resistors bridge (in Fig. 18.23, indicated as PZR) imposes the deposition of an insulant layer (like silicon dioxide) and the realization of a local interconnection layer in metal (in Fig. 18.23b, the orange layer). The choice of the right metal material will be done

by considering the desired series resistance and the ohmic behaviour of the contact. After the local interconnection realization, a passivation layer (like Silicon Nitride or Silicon Oxi-nitride) is deposited on top of it (Fig. 18.23c, cyan layer). Vias in passivation layer to reach the local interconnection can be opened by using a dry etch or a wet etch.

The following step is the deposition of a seed metal layer for the coil growth. In order to have the highest force, and to reduce consumption related to power dissipation, the coil has to be long with low resistance. To match these requirements, the electrochemical deposition is the preferred technique to realize such metallization. On metal seed layer, a mask is realized by using lithography, then the ECD growth is performed. After the growth, the photoresist is stripped, and the seed layer is removed by wet chemical etch. The seed material must match the wettability requirement for the electrochemical growth, while the coil material has to have the lowest resistance value. The preferred material for coil and seed are copper or gold.

In Fig. 18.23c, it is shown the sequence of the described steps. Since the longest the coil is, the stronger is the force, a very compact wire layout must be realized on silicon. To match 720p resolution target, the coil thickness must be greater than 25 μm and the coil pitch around 30 μm, where the space is reduced to a half respect the metal width. In such situation, the photoresist during the growth is stressed, and a smart layout and a robust process window is needed to avoid line collapse, which can have a detrimental effect on force.

In Fig. 18.24, the completed mirror device is shown.

If copper is used as metal material for coil, sometimes a top finishing with nickel is introduced to protect the wire top from oxidation, as shown in Fig. 18.25.

By depending on mirror design, Bi-axial or mono-axial, a second thick metal layer (realized by ECD) with low resistance can be necessary to manage the coil current signal. For Bi-axial design, this second interconnection has to pass over one
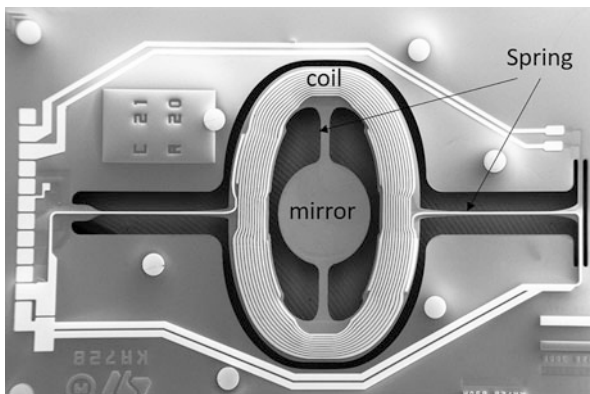

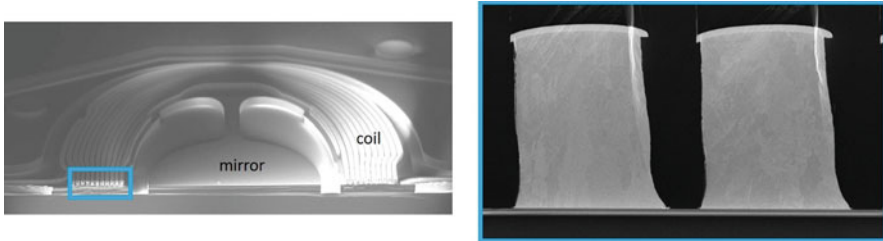**Fig. 18.24** Electromagnetic mirror. SEM picture of the final device

Fig. 18.25 SEM cross section of the COIL of electromagnetic Mirror

of the axes springs. In this arrangement, such metallization must be robust enough to sustain the stress coming from mirror movement in both directions. Gold and copper are ductile material, and they are not suitable to ensure the desired lifetime. Other metals and alloys with better resistance to damage and breakage under movement must be used.

After thick metal realization, the mirror surface can be cleaned from dielectric and the mobile mass is defined through lithography and silicon dry etch (Fig. 18.23 d).

In order to match high-resolution target, the mirror mechanical angle has to be as high as possible especially for horizontal scanning, as result the operative stress in silicon can be close to 1GPa. To sustain such stress level in operating condition, the silicon of the spring has to be free of crystal or other defects as explained in [22]. Since dry silicon etch can create some crystal damages on the sidewall, after the mobile mass definition, it is suggested to remove the damaged area, by using an isotropic silicon etch [23]. Dry (SF6 or CF4) or wet (TMAH or KOH) etch can be used for this purpose [24].

The mirror release (Fig. 18.23 e) is performed by using a backside mask and dry silicon etch. As previously commented, the front to back operation can cause severe damage of the wafer frontside and a front side protection is necessary. Respect to electrostatic case, in this process scheme, at this step, the topography present on the wafer front can be important and the chosen front side protection has to be able to manage up to 60 μm of height difference between the top of the coil and the buried oxide. Since the Lorenz force is stronger as the closer is the permanent magnet to the coil, depending on the magnet arrangement in the final package, the handle silicon can be reduced in thickness down to 120 μm. To manage such thin-holed wafer, a carrier wafer is mandatory. With backside mask and etch, a reinforcement under the mirror or coil can be realized, if the design requires it.

The reflective surface is realized as the final step of the flow, by metal deposition through a shadow mask.
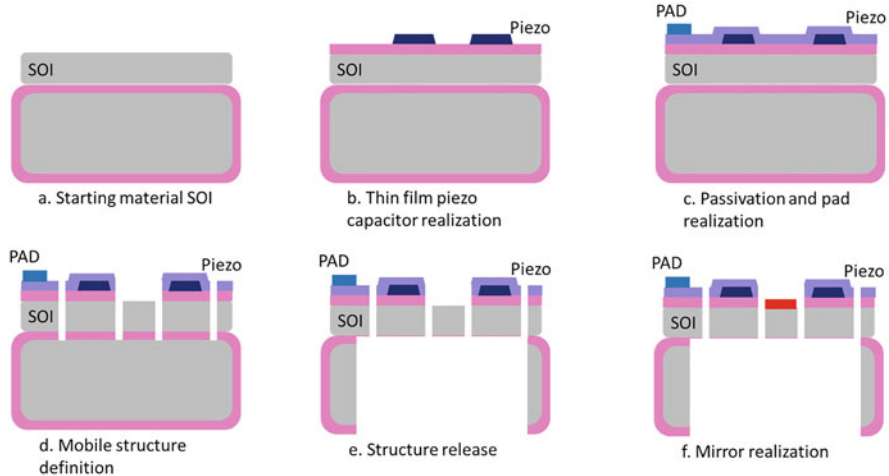
Fig. 18.26 Schematic process flow for thin film piezo actuated Mirror: (**a**) starting material, (**b**) thin film piezo capacitor realization, (**c**) passivation and pad realization, (**d**) mobile structure definition, (**e**) structure release, (**f**) mirror realization

18.4.3 Thin-Film Piezo Technology

Thanks to the availability in semiconductor facilities of equipment able to perform a thin-film piezo deposition on silicon wafer (by sputtering or solgel coating) some devices, like micromirrors, can benefit of this strong actuation principle.

The thin-film piezo mirror technology consists of the realization of a reflective surface, the mobile structure and the thin-film piezo actuator over a thin silicon cantilever.

In Fig. 18.26, a schematic sequence of the major process flow steps necessary to mirror realization is shown.

Like electromagnetic mirror, the sensing of the mirror position has to be performed by using a piezo-resistance bridge or by using the thin-film piezo itself, if its current versus voltage characteristic is linear and stable enough. In Fig. 18.26, the realization of the sensing part is not reported. Starting from an SOI wafer, an isolation layer like silicon dioxide is deposited on silicon surface in order to insulate piezo capacitor from substrate. After such dielectric deposition, the thin-film piezo stack (bottom electrode, piezo material and top electrode) is realized by using standard deposition technique (sputtering PVD or solgel).

The actuators are then defined through photo lithography and etch (Fig. 18.26b): dry or wet chemistry can be used. After capacitor patterning, a dielectric passivation layer is deposited on top. If lead–titanate–zirconate material is used as actuator, the passivation material or passivation stack has to avoid the usage of Hydrogen close to piezo material, since it has a detrimental effect on piezo performance [25]. After passivation deposition, vias are opened in dielectric material with photolithography

Fig. 18.27 PZT actuated quasi-static mirror. SEM picture

and etch, to reach capacitor electrode. A metal layer is deposited to realize the electrical contact to piezo, the interconnection and the pad (Fig. 18.26c).

The dielectric over the mirror surface can be removed using Via mask or after metal patterning, however before mobile structure definition with lithography and dry etch (Fig. 18.26d). Dry silicon etch is used to keep the sharp profile on the spring and the removal of the damaged silicon sidewall is suggested also for this technology if the device performance and reliability require it.

The mirror release and the reflective surface realization follow the steps described in the previous paragraphs. To have an effective actuation, during back-side silicon etch, the silicon handle layer has to be removed also from the back of the piezo cantilever (as shown in Fig. 18.26e), in order to have the maximum structure deflection and mirror rotation. In Fig. 18.27, the SEM picture of PZT actuated mirror is shown. The four thin-film piezo capacitors are disposed in a symmetric way respect to the central mirror, as explained in Fig. 18.16. In Fig. 18.28, other examples of piezo-actuated micromirrors are reported.
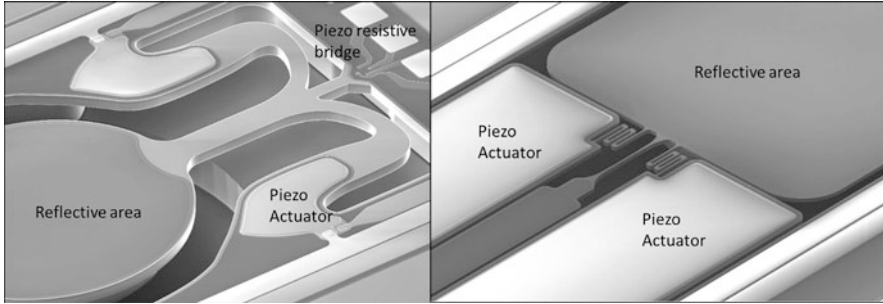
Fig. 18.28 Details of thin-film Piezo actuated mirrors (SEM picture). Resonant (on the left side) and quasi-static mirror (on the right side) are shown

18.4.4 Reflective Surface: Requirements and Realization

In the previous paragraphs, the realization of the mobile structure is widely described, but the reflective surface has been treated in a marginal way. The aim of this section is to describe more in detail that part. In portable projection system, a great effort is spent to minimize consumption: the final image brightness and contrast are directly related to laser power and the loss/light adsorption in optical path has to be avoided as much as possible. To have a more effective system, the mirror reflectance has to be the highest possible (>90%). With such constraint, the silicon itself, even with a high doping level, cannot be a powerful reflective surface and a metal layer is mandatory.

Let's split the reflective surface versus the application: if the final target is projection, that means visible (VIS) region (400–635 nm), silver or aluminium is the best choice, while for gesture recognition, that means infrared (800–1000 nm), the gold is the preferred material. The reason is that aluminium and silver have a flat reflectivity response along all the visible range, whereas gold has very high reflectivity but only for wavelengths higher than 600 nm.

Aluminium, gold and silver are material that can be deposited in thin film by evaporation or sputtering PVD and are present in a semiconductor factory, with a high purity grade.

In Fig. 18.29, the reflectance characteristics of pure aluminium, silver alloy and pure gold thin film (thickness less than 300 nm), collected with a double beam reflectometer at quasi normal incidence (9 degree), is shown. The data are well aligned to the ones available in literature [26] .

To reach the desired optical performance, the roughness of the metal layer must be the lowest possible (Rms < 10 nm). This imposes the usage of polished grade surface as starting material for reflective surface realization: for example, mono-silicon is preferred to epipoly silicon even after CMP. The silicon surface must be free of defects (like scratches), and oxide wet etch is preferable to dry oxide etch to clean silicon surface before metal deposition.
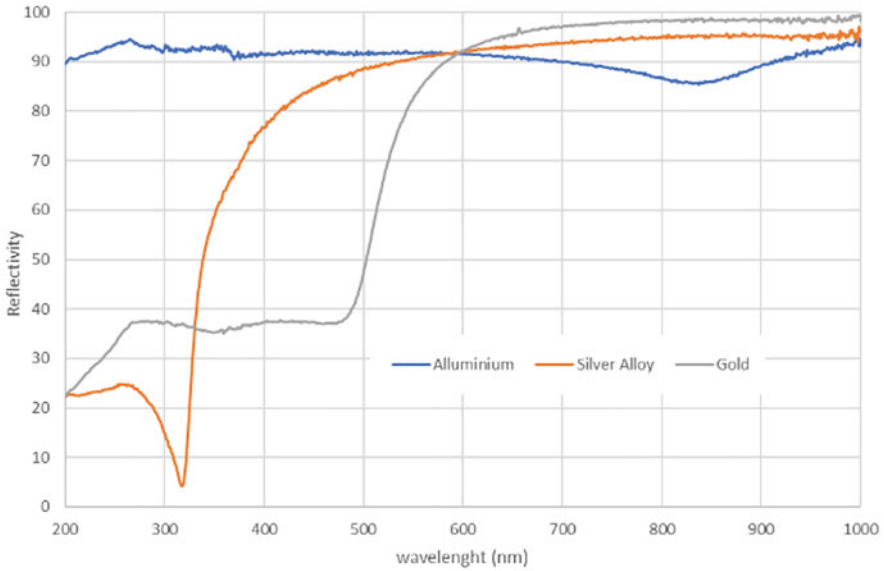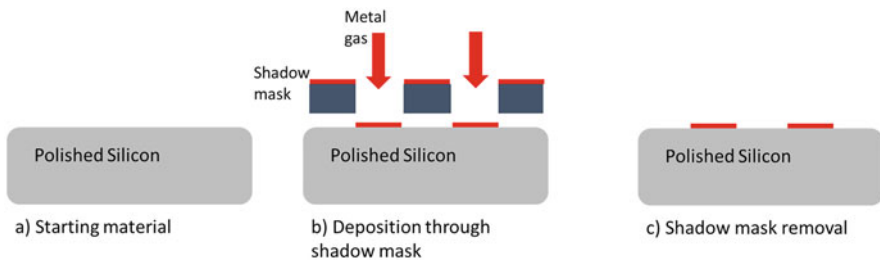
Fig. 18.29 Metal thin-film reflectance spectra

Fig. 18.30 Shadow mask approach. Mirror realization: (**a**) starting material, (**b**) deposition through shadow mask, (**c**) shadow mask removal

Between metal and silicon, a barrier or an adhesion layer can be present in order to guarantee metal adhesion and to avoid diffusion of metal in silicon, that can cause defects.

There are two possible ways to realize the metal of the mirror: the first is the one suggested in the process flows described before, the deposition through a shadow mask, and the second is the full sheet metal deposition followed by a patterning through photolithography and etch. The two methods are explained in Figs. 18.30 and 18.31.

Shadow mask is a technique widely used in research centres and universities, where it is often performed in a manual arrangement: it is cheap, it has an high flexibility – since it can be applied to released structure – but the drawback is the poor thickness uniformity of the deposited material due to the shadow effect. As
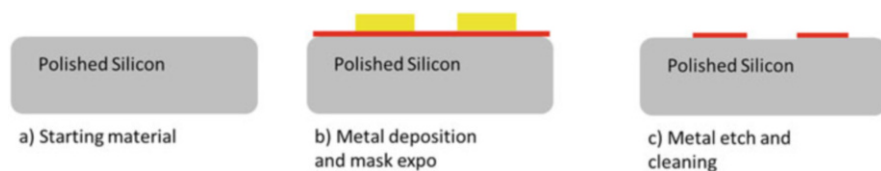
Fig. 18.31 Mirror realization with full sheet approach: (**a**) starting material, (**b**) metal deposition and mask expo, (**c**) metal etch and cleaning

described in [27], the shadow mask wall blocks a part of metal deposition and creates a "dome-shaped" metal profile. Such dome profile can be minimized, by reducing shadow mask thickness, but it can never be completely suppressed.

The "dome profile" contributes to the static curvature of the mirror: by increasing system resolution, this time zero distortion must be limited as much as possible.

Full sheet approach is more expensive and imposes a more complex integration. The plus respect to shadow mask is that the mirror static curvature is related only to mechanical design and to metal film stress control.

Since metal reflectivity is directly related to image brightness and contrast, it has to be as higher as possible in order to reduce laser power consumption. For such reason, in visible range, silver is preferable to aluminium, due to superior optical performance, but the usage of silver usually imposes the adoption of protective coating since the material is prone to tarnish. The adoption of an optical coating for protection and for reflectivity enhancement is something widely used in optics. The thickness and the material choice (in terms of refractive index) is optimized in order to minimize or to improve the impact on optical response. This technique can be also applied in MEMS micromirror as described in [28, 29]. For protection coating, in the visible range, the best choice is the mono-silicon oxide (SiO), and for enhancement coating, an alternate sandwich of low refraction index and high refraction index material is usually applied, as shown in Fig. 18.32. As low refraction index silicon dioxide (n = 1.46 at 632 nm [30]) is a good choice, while for high refraction index, Al_2O_3 (n = 1.77 at 632 nm [30]), HfO_2 (n = 1.91 at 632 nm [30]) or Nb_2O_5 (2.32 at 632 nm [30]) can be good alternatives. All these materials can be easily found in a semiconductor front end fab.

The thickness of the material is a fraction of used wavelength (usually λ/4), in order to take advantage from constructive interference. The exercise of enhancement reflectivity, widely used in optics, is more complex in scanning micromirror, since the optical path of the incident light is a function also of scanning angle.

In pico-projection application, sometimes there is another optical requirement: to have all the "non-reflective surfaces" as dark as possible, to suppress all the unwanted reflection coming from MEMS fixed part. This kind of defect is called "stray light" and it is related to wide tolerance of alignment of laser beam inside the optical module. Two ways are possible to realize a non-reflective surface on the MEMS from technology point of view: the first is the deposition of a dark coating upon the fixed surface, and the second is to realize a very rough surface that creates
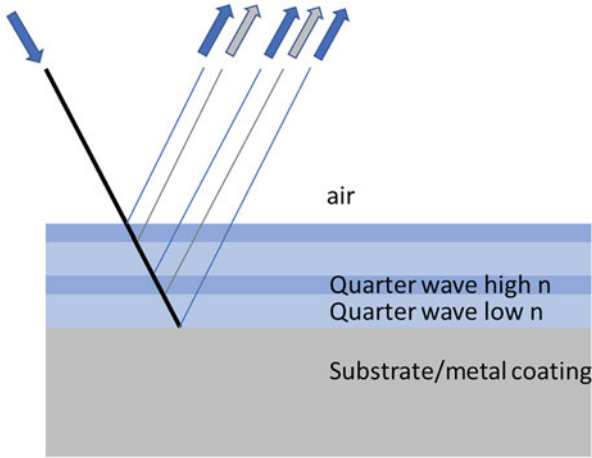
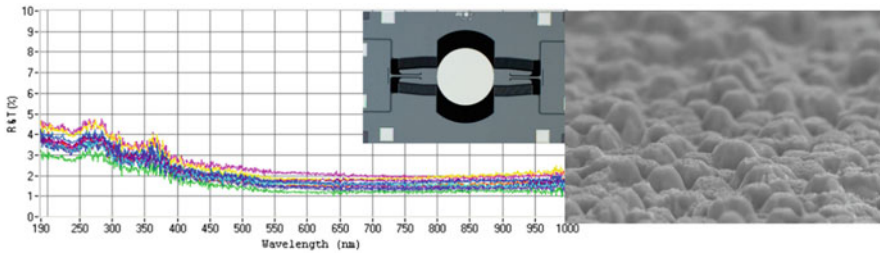**Fig. 18.32** Schematic quarter wave stack for enhanced reflectivity

Fig. 18.33 Resonant Electrostatic Mirror with black cavity (reflectivity spectra and SEM picture details of the black surface)

a high level of absorption, like what happens in moth's eyes. In Fig. 18.33, it is shown the realization of a black surface in the cavity where the mirror moves with the reflectivity spectra.

18.4.5 Process Specificities: Vacuum Usage for Improved Performance and Reliability

To suppress air damping effects, the usage of hermetic vacuum package is suggested. The reduced atmosphere improves mirror performance and reduces consumption since higher aperture can be reached with lower power. For electrostatic mirror, it is possible to reduce the extension of comb-drive area since the force in vacuum is more effective [31]. Fraunhofer Institute worked on this approach at wafer level for electrostatic biaxial mirror [19], and showed that 15 degree of
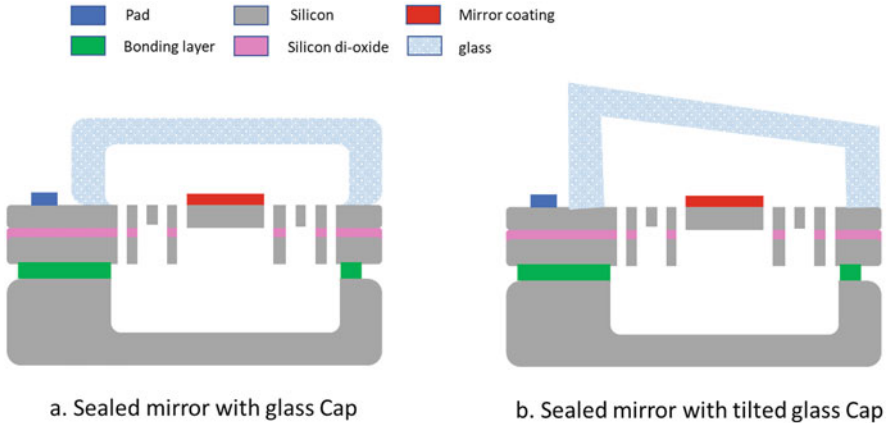
Fig. 18.34 Hermetic electrostatic mirror cross section: (**a**) sealed mirror with glass cap, (**b**) sealed mirror with tilted glass cap

mechanical angle on fast resonant axis can be reached with a pulse of 60 V instead of 200 V. The solution presented by Fraunhofer used Titanium Getter to reduce inner pressure down to 0.1 Pa.

The solution of vacuum sealing at wafer level is a technology widely used for MEMS gyroscope, even if in the case of scanning micromirror is more complex, since it requires the usage of three wafers instead of two, and the usage of glass wafer to allow the light transmission.

Regarding to device layout, the scanning mirror has to be surrounded by a closed frame, with minimum topography in order to allow the hermetic W2W bonding. For electrostatic mirror, the connection to stator and rotor electrical domain has to be performed with buried polysilicon connection, as explained in [19] and the process flow can be further complicated by using vertical separation trenches filled by insulator as described in [32]. In Fig. 18.34, a schematic cross view of final device is shown.

The sensor wafer, the one where the mechanical mirror structure is realized, is bonded to a support silicon wafer where a deep cavity is realized by using W2W bonding technique like glassfrit or metallic bonding (e.g. Au-Au). The top cap wafer is made up with glass with several cavities to allow the mirror rotation and it is bonded to the sensor wafer by using glassfrit or anodic bonding. The bonding sequence can be reversed with respect to the flow here described and a getter can be deposited on support wafer through lift-off or shadow mask, if it is required to reach the desired vacuum level and device lifetime.

The usage of the glass in the architecture proposed in Fig. 18.34a has one drawback: the formation of a white spot at the centre of the projected field due to the glass surface back reflection, as explained in [19]. This spurious effect can be avoided by using an antireflective coating on the glass surface or using a tilted glass in order to shift the reflection out of the projection path, as shown in Fig. 18.34b.

Fraunhofer Institute suggested 15 degree of tilting good enough to suppress the white spot [19]. The method of realization of a glass wafer with such characteristics can involve micromachining technique and it is described in [33].

Vacuum and hermetic sealing guarantee better lifetime, since the MEMS device is not exposed to humidity, dust and aggressive contaminants present in air.

References

1. Petersen, K. E. (1980). Silicon torsional scanning mirror. *IBM Journal of Research and Development*, 631–637.
2. [Online]. Available: https://en.wikipedia.org/wiki/Digital_micromirror_device
3. Nelson, P. White Paper – DLP technology for spectroscopy, February 2014. [Online]. Available: https://www.ti.com/lit/wp/dlpa048a/dlpa048a.pdf
4. Urey, H., et al. (2000). Optical performance requirements for MEMS-scanner based microdisplays. *Conference on MOEMS and Miniaturized Systems, SPIE, 4178*, 176–185.
5. [Online]. Available: microvision.com/sony-mp-cl1-pico-projector-announcement/
6. [Online]. Available: https://www.theverge.com/2019/2/24/18235460/microsoft-hololens-2-price-specs-mixed-reality-ar-vr-business-work-features-mwc-2019
7. Holmstrom, S., et al. (2014). MEMS laser scanners: A review. *Journal of Microelectromechanical Systems*, 259–275.
8. Wu, L., & al. (2010). A tip-tilt-piston micromirror array for optical phased Array applications. *Journal of Microelectromechanical Systems, 19*(6), 1450–1461.
9. Inagaki, S., et al. (2019). High resolution piezoelectric MEMS scanner fully integrated with focus-tuning and driving actuators. In *Transducers 2019 – EUROSENSORS XXXIII, Berlin, Germany*.
10. Zhang, X., et al. (2001). A study of the static characteristics of a torsional micromirror. *Sensors and Actuators A*, 73–81.
11. Song, Y., et al. (2018). A review of micromirror arrays. *Precision Engineering, 51*, 729–761.
12. Yalcinkaya, A., & al. (2007). NiFe plated biaxial MEMS scanner for 2-D imaging. *IEEE Photonics Technology Letters, 19*(5), 330–332.
13. Hsu, S., et al. (2008). Two dimensional microscanners with large horizontal-vertical scannng frequency ration for high resolution laser projectors. In *Proceedings of SPIE*.
14. Yalcinkaya, A., et al. (2006). Two-Axis electromagnetic microscanner for high resolution displays. *Journal of Microelectromechanical Systems, 15*(4), 786–794.
15. Genenko, Y. A., et al. (2015). Mechanisms of aging and fatigue in ferroelectrics. *Materials Science and Engineering B*, 52–82.
16. Boni, N., Carminati, R., Mendicino, G., & Merli, M. (2021). Quasi-static PZT actuated MEMS mirror with 4x3mm2 reflective area and high robustness. In *Proceedings of SPIE 11697, MOEMS and Miniaturized Systems XX, 1169708*.
17. Schneider, R. (2016). *High-Q AlN contour mode resonators with unattached, voltage-actuated electrodes,* Graduate thesis in Electrical Engineering and Comuputer Sciences, University of California at Berkeley.
18. Arslan, A., Brown, D., Davis, W. O., & al. (2010). Comb-actuated resonant torsional microscanner. *Journal of Microelectromechanical Systems, 19*(4), 936–943.
19. Hoffman, U., Eisermann, C., & Quenzer, H.-J. (2011). MEMS scanning laser projection based on high-Q vacuum packaged 2D-resonator. In *SPIE – The International Society for Optical Engineering 7930*.
20. Kim, M. (2009). High fill-factor micromirror array using a self-aligned vertical comb drive actuator with two rotational axes. *Journal of Micromechanics and Microengineering, 19*, 035014 (9pp).

21. Ataman, C., et al. (2013). A dual-axis pointing mirror with moving-magnet actuation. *Journal of Micromechanics and Microengineering, 23*, 025002 (13pp).
22. Gaither, M. S., Gates, R. S., Kirkpatrick, R., Cook, R. F., & DelRio, F. (2013). Etching process effects on surface structure, fracture strength, and reliability of single-crystal silicon theta-like specimens. *Journal of Microelectromechanical Systems, 22*(3), 589–602.
23. Noonan, E. E., et al. (2008). The scaling of strength in the design of high-power MEMS structures. *Scripta Materialia, 59*(9), 927–930.
24. Tilli, M., Motooka, T., Airaksinen, V. M., Franssila, S., Paulasto-Krockel, M., & Lindroos, V. (2015). Chapter 21 – Deep reactive Ion etching. In *Handbook of silicon based MEMS materials and technologies-second edition* (pp. 464–465). William Andrew – Elsevier.
25. Seo, S., Yoon, J., Song, T. K., Kang, B. S., & Noh, T. W. (2002). Mechanism of low temperature hydrogen-annealing-induced degradation in Pb(Zr 0.4 Ti 0.6)O3 Capacitors. *Applied Physics Letters, 81*(4), 697–699.
26. Paquin, R. A. (1995). Chapter 35: Properties of metals. In *Handbooks of optics-volume II* (pp. 35.30–35.39). New York: McGraw-Hill.
27. Yao, S. K. (1979). Theoretical model of thin-film deposition profile with shadow effect. *Journal of Applied Physics, 50*, 3390–3395.
28. Zannuccoli, M., et al. (2017). Simulation of micro-mirrors for optical MEMS. In *SISPAD Proceedings*.
29. Cianci, E., et al. (2018). Advanced protective coatings for reflectivity enhancement by low temperature atomic layer deposition of HfO2 on Al surfaces for micromirror applications. *Sensor and Actuators A: Physical, 282*, 124–131.
30. FILMETRICS: Refractive index database. Filmetrics, [Online]. Available: https://www.filmetrics.com/refractive-index-database. Accessed 29 Mar 2020.
31. Manh, C. H., & Hane, K. (2009). Vacuum operation of comb-drive micro display mirrors. *Journal of Micromechanics and Microengineering, 19*, 105018–105026.
32. Schenk, H., Durr, P., Kunze, D., Lanker, H., & Kuck, H. (2001). A resonantly excited 2D-micro-scanning-mirror with large deflection. *Sensors and Actuators A, 89*, 104–111.
33. Merz, P., Quenzer, H. J., Bernt, H., Wagner, B., & Zoberbier, M. (2003). A novel micro-machining technology for structuring borosilicate glass substrates. In *The 12th international conference on solid state sensors*. Boston: Actuators and Microsystems.